Electron-electron interactions in the nonparabolic conduction band of narrow-gap semiconductors

Michael P. Hasselbeck* and Peter M. Enders†
Max-Born-Institut für Nichtlineare Optik und Kurzzeitspektroskopie, D-12489 Berlin, Germany
(Received 15 December 1997)

The Lindhard dielectric function is evaluated at nonzero temperatures with Fermi-Dirac statistics and a nonparabolic conduction band for bulk, narrow-gap semiconductors. This is used to study two problems of current interest: (i) inelastic scattering of single, energetic electrons by a system of plasmons, phonons, and quasiparticle excitations; and (ii) cooling of a hot, quasiequilibrium plasma by dynamically screened LO-phonon emission. Scattering of high-energy electrons injected into *n*-doped InAs at room temperature is analyzed and compared to the case where nonparabolicity is neglected. Plasmon losses and a larger density of states are shown to be more important for electrons in a nonparabolic conduction band with energy above the Fermi level. The energy-loss rate of a hot-electron–donor ion plasma to a cold lattice via screened LO-phonon emission in parabolic and nonparabolic bands is also obtained. It is found that even though dynamic screening of LO phonons is stronger in a nonparabolic band, the cooling rate of hot electrons in InAs can be significantly faster because of the increased density of conduction-band states.
[S0163-1829(98)04916-9]

I. INTRODUCTION

The interaction of free electrons in the conduction band of semiconductors is of considerable interest for device applications as well as understanding fundamental carrier dynamics.[1] It is especially relevant when dimensions are small and/or carrier concentrations are high. Despite the technological significance of narrow-gap semiconductors, however, a finite-temperature treatment of the electronic susceptibility in a nonparabolic conduction band has not been available. Dingrong *et al.*[2] considered the electron-electron interaction in narrow-gap semiconductors at zero temperature for two restricted cases: (i) light doping with a parabolic band, and (ii) heavy doping and a linear band. Coupling of longitudinal plasma oscillations to phonons was neglected. These limitations are removed here to allow for a more realistic description of experiments at elevated temperature where practical devices operate. A Fermi-Dirac distribution of conduction electrons (not necessarily at the lattice temperature) is used throughout.

The central theme of this paper is assessing the influence of nonparabolicity compared to the usual parabolic approach for analysis of intraband scattering. Nonparabolicity affects the inelastic scattering of electrons in a variety of ways such as: (i) increased density of states, (ii) changes to the conditions for energy and momentum conservation, (iii) reduction of Bloch function matrix elements, and (iv) changes in the dynamic interplay between lattice and electronic components of the semiconductor susceptibility. These effects tend to be interrelated and can be difficult to isolate. The specific situations examined here, however, allow some general conclusions to be drawn—foremost being that the increased density of states in a nonparabolic band makes the scatter rate higher compared to a parabolic band with equivalent electron density and temperature. The other aspects of the problem play a less important role.

This paper is organized as follows. The scatter spectrum of the coupled plasmon-phonon system is obtained as a function of frequency and wave vector. This is used to investigate inelastic collisions in two situations where nonparabolicity is relevant. Scattering of energetic electrons injected into *n*-doped InAs, which has implications for room-temperature operation of unipolar ballistic electron transistors and resonant-tunnel diodes, is examined in Sec. III. The effect of nonparabolicity on the cooling of an (optically heated) electron-donor ion plasma by screened phonon emission is considered in Sec. IV.

II. LINDHARD FUNCTION

In Kane's semiconductor band theory, the conduction band is reasonably approximated as isotropic but nonparabolic.[3] The dispersion relation for conduction electrons is

$$\frac{\hbar^2 k^2}{2m} = \gamma(E) = E(1+\alpha E), \tag{1}$$

where $\alpha = 1/E_g$, and m is the band-edge electron effective mass. The effect of nonparabolicity is illustrated in Fig. 1, where the room-temperature dispersion near the center of the Brillouin zone is plotted for the narrow-gap semiconductors InSb ($E_g = 0.18$ eV) and InAs ($E_g = 0.36$ eV), assuming both parabolic ($\alpha = 0$; dashed lines) and nonparabolic bands (solid lines). The bottom of the conduction band is taken as zero energy. The insets depict the density of states as a function of electron energy for the two different cases. As conduction electrons acquire energy that is an increasing fraction of the band-gap energy, the parabolic approximation becomes progressively poorer. From this picture, it is clear that nonparabolicity should be accounted for when degenerate concentrations and elevated temperatures are encountered—exactly the situation found in many types of electronic devices with *n*-doped regions of InAs.

The random-phase approximation allows the total dielectric function of the semiconductor to be written as the sum of lattice, free carrier, and background contributions:[1]

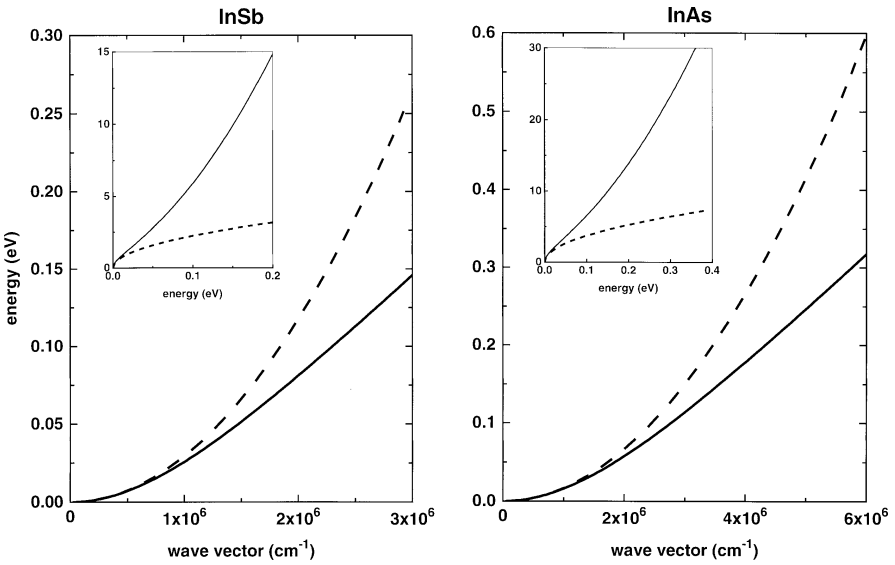

FIG. 1. Conduction bands of InSb and InAs at room temperature assuming parabolic dispersion (dashed lines) and Kane's nonparabolic relation (solid line). Only a small region near the center of the Brillouin zone is shown. The insets depict the density of states (in arbitrary units) as a function of conduction-electron energy (dashed lines for parabolic; solid lines denote nonparabolic).

$$\varepsilon(q,\omega)=\Delta\varepsilon_L(\omega)+\Delta\varepsilon_e(q,\omega)+\varepsilon_\infty, \tag{2}$$

where the lattice term is

$$\Delta\varepsilon_L(\omega)=\frac{\varepsilon_0-\varepsilon_\infty}{1-\left(\frac{\omega}{\omega_{\mathrm{LO}}}\right)^2\frac{\varepsilon_0}{\varepsilon_\infty}}. \tag{3}$$

The bare phonon frequencies are assumed to be dispersionless in this paper. Free holes are not included as the focus is on electron-donor ion plasmas encountered in single-carrier optical experiments and electronic devices. Contributions from the valence bands, which would be important in optical excitation of electron-hole pairs in lightly doped material for example, can be incorporated following Refs. 4–6. The susceptibility of the conduction electrons is obtained from the Lindhard formula for the dielectric function[7]

$$\Delta\varepsilon_e(q,\omega)=\frac{4\pi e^2}{q^2}\sum_{\mathbf{k}} f(k)\left[\frac{I^2_{\mathbf{k},\mathbf{k}+\mathbf{q}}}{E_{\mathbf{k}+\mathbf{q}}-E_{\mathbf{k}}-\hbar\omega-i\hbar\Gamma}+\frac{I^2_{\mathbf{k},\mathbf{k}-\mathbf{q}}}{E_{\mathbf{k}-\mathbf{q}}-E_{\mathbf{k}}+\hbar\omega+i\hbar\Gamma}\right] \tag{4}$$

where $f(k)$ is the Fermi-Dirac function and Γ is a phenomenological damping term. Wave-function overlap factors appropriate for intraband transitions in a nonparabolic conduction band are used:[8]

$$I^2_{\mathbf{k},\mathbf{k}\pm\mathbf{q}}=\frac{\left[\sqrt{(1+\alpha E_{\mathbf{k}})(1+\alpha E_{\mathbf{k}\pm\mathbf{q}})}+\alpha\sqrt{E_{\mathbf{k}}E_{\mathbf{k}\pm\mathbf{q}}}\cos\,\vartheta_{\mathbf{k},\mathbf{k}\pm\mathbf{q}}\right]^2}{(1+2\alpha E_{\mathbf{k}})(1+2\alpha E_{\mathbf{k}\pm\mathbf{q}})}. \tag{5}$$

In Eq. (5), $\vartheta_{\mathbf{k},\mathbf{k}\pm\mathbf{q}}$ represents the angle between the initial-state ($\mathbf{k}$) and final-state ($\mathbf{k}\pm\mathbf{q}$) wave vectors, with $\mathbf{q}$ denoting the wave vector of the scattered particle. When the sum in Eq. (4) is converted to an integral, the z axis is fixed in the direction of $\mathbf{q}$. The polar integration coordinate becomes θ, which is the angle between $\mathbf{k}$ and $\mathbf{q}$. Therefore, the substitution

$$\cos\,\vartheta_{\mathbf{k},\mathbf{k}\pm\mathbf{q}}=\left(\frac{\gamma(E_k)}{\gamma(E_{\mathbf{k}\pm\mathbf{q}})}\right)^{1/2}\left[1\pm\left(\frac{q}{q_o}\right)\left(\frac{\hbar\omega_{\mathrm{LO}}}{\gamma(E_k)}\right)^{1/2}\cos\,\theta\right] \tag{6}$$

is made, where the normalizing parameter q_o is introduced:

$$q_o=\frac{\sqrt{2m\hbar\omega_{\mathrm{LO}}}}{\hbar}. \tag{7}$$

The energy of the final state is written

$$E_{\mathbf{k}\pm\mathbf{q}}=\frac{1}{2\alpha}\left\{-1+\left[1+4\alpha\gamma(E_k)+4\alpha\left(\frac{q}{q_o}\right)^2\hbar\omega_{\mathrm{LO}}\pm 8\alpha\sqrt{\gamma(E_k)\hbar\omega_{\mathrm{LO}}}\left(\frac{q}{q_0}\right)\cos\,\theta\right]^{1/2}\right\}, \tag{8}$$

allowing Eq. (4) to be re-expressed as the following double integral:

$$\Delta\varepsilon_e(q,\omega)=\frac{\sqrt{2m}}{\pi\hbar}\frac{e^2}{\left(\frac{q}{q_o}\right)^2\hbar\omega_{\mathrm{LO}}}\int_{-1}^{1}d(\cos\,\theta)\times\int_0^\infty dE\; f(E)\sqrt{\gamma(E)}(1+2\alpha E)\times\left[\frac{I^2_{\mathbf{k},\mathbf{k}+\mathbf{q}}(\cos\,\theta,E)}{E_{\mathbf{k}+\mathbf{q}}(\cos\,\theta,E)-E-\hbar\omega-i\hbar\Gamma}+\frac{I^2_{\mathbf{k},\mathbf{k}-\mathbf{q}}(\cos\,\theta,E)}{E_{\mathbf{k}-\mathbf{q}}(\cos\,\theta,E)-E+\hbar\omega+i\hbar\Gamma}\right]. \tag{9}$$

Following the usual procedure, the radial k coordinate has been replaced by $E_{\mathbf{k}}$. The vector nature of the scattering

collisions has been accounted for at this point, so the subscript on E_k can be dropped. Note that the conduction band is taken to be isotropic, so $\Delta\varepsilon_e$ depends only on the modulus of $\mathbf{q}$.

The zeros of $\varepsilon(q,\omega)$ belong to plasmons exhibiting oscillations of frequency $\omega_p(q)$. In infrared reflection experiments, the long-wavelength limit ($q\rightarrow 0$) is measured. In this limit and neglecting damping ($\Gamma=0$), Eq. (2) can be written in general as

$$\varepsilon(0,\omega)=\Delta\varepsilon_L(\omega)+\varepsilon_\infty\left(1-\frac{\omega_p^2}{\omega^2}\right). \tag{10}$$

Here ω_p is the modified Langmuir plasma frequency

$$\omega_p^2=\frac{4\pi e^2 N}{m(N)\varepsilon_\infty}, \tag{11}$$

where the optical mass $m(N)$ accounts for the nonparabolic dispersion of a conduction band with electron density N:[9]

$$\frac{1}{m(N)}=\frac{1}{12\pi^3\hbar^2 N}\int d\mathbf{k}\,\frac{\partial^2 E}{\partial k_x^2}\,f(E). \tag{12}$$

For the nonparabolic band considered here, this becomes

$$\frac{1}{m(N)}=\frac{\sqrt{2m}}{\pi^2\hbar^3 N}\int_0^\infty dE\; f(E)\sqrt{\gamma(E)}\left(1-\frac{4}{3}\,\frac{\alpha\gamma(E)}{(1+2\alpha E)^2}\right). \tag{13}$$

The plasma frequency is then easily found by inserting Eq. (13) into Eq. (11). This, of course, reduces to the classical Drude result when $\alpha=0$. Equation (13) can also be obtained directly by taking the limit $q\rightarrow 0$ in Eq. (9). The free carrier density is given by the integral

$$N=\frac{\sqrt{2}m^{3/2}}{\pi^2\hbar^3}\int_0^\infty dE\; f(E)\sqrt{\gamma(E)}(1+2\alpha E). \tag{14}$$

The optical mass $m(N)$ describes the dispersion of an equivalent *parabolic* band, which is implicit in the Drude model. Plasma oscillations involve electrons in all regions of k space determined by the Fermi distribution function. An increase of $m(N)$ with doping, as is known from infrared reflectivity measurements,[9,10] manifests the fact that a higher percentage of electrons occupy regions of the conduction band with decreasing curvature. Here is an important difference with the situation in a classical (parabolic) band: the plasma frequency is altered when either the density or temperature of the carriers changes.

In Fig. 2, reflectivity resonances obtained from Spitzer and Fan's room-temperature InSb data are shown.[9] The plotted points are nulls in the spectra that occur when the dielectric function makes the normal-incidence Fresnel reflectivity vanish [i.e., at $\varepsilon(\omega)=1$]. These points are in close proximity to (but not identically equal to) the upper-hybrid modes of the coupled plasmon-phonon system. The reflectivity nulls in Fig. 2 are seen to agree with a calculation (solid line) using Eqs. (10), (11), and (13), and established parameters for room-temperature InSb ($m=0.013m_o$, $E_g=0.18$ eV, $\hbar\omega_{\rm LO}=0.023$ eV, $\varepsilon_0=17.54$, and $\varepsilon_\infty=15.68$). Also shown is the case where nonparabolicity is neglected (dashed line).

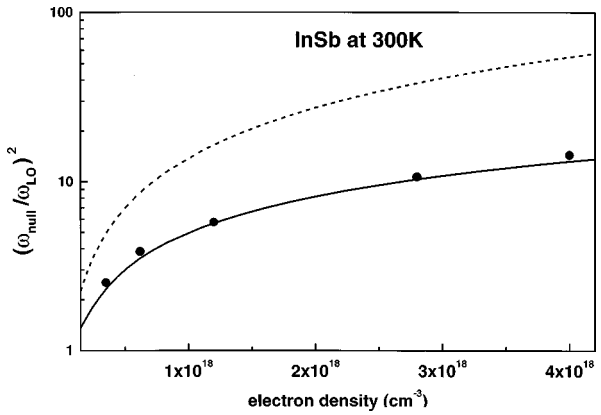

FIG. 2. Nulls in the infrared reflection spectrum of room-temperature n-doped InSb as a function of doping. Plotted points are taken from the data of Spitzer and Fan (Ref. 9), normalized to the LO-phonon frequency. The curves are obtained from Fresnel reflectivity calculations using the dielectric function $\varepsilon(0,\omega)$ for a nonparabolic (solid line) and parabolic (dashed line) conduction band.

The emphasis of this paper is on understanding the effect of band nonparabolicity on the frequency- and momentum-dependent scatter spectrum of the system. This is given by the imaginary part of the reciprocal dielectric function, $\mathrm{Im}(1/\varepsilon(q,\omega))$, requiring that Eq. (9) be evaluated at all values of q.[1,7,8] The usual procedure is to let $\Gamma\rightarrow 0$, compute the real part of $\Delta\varepsilon_e$, and then obtain the imaginary portion by a Kramers-Kronig transformation. In this work, Γ is retained, which allows Eq. (9) to be separated into real and imaginary components that are integrated independently. Including damping is mathematically convenient because it prevents singularities at the plasmon pole, but requires that a value of Γ be specified. For the doping densities considered here, $\hbar\Gamma\ll\hbar\omega_{\rm LO}$, $\hbar\Gamma\ll\hbar\omega_p$, which is manifest by sharp nulls seen in the reflectivity data in Refs. 9 and 10. To satisfy this inequality, Γ is set at 5×10^{12} s^{-1} in the present calculations. Similar numbers have been used in previous treatments of Γ in the complex dielectric function.[11–13] This term, however, should not be understood as the collisionally broadened linewidth of the electron-electron interaction, as pointed out by Mermin.[14] For the situations analyzed in this paper, plasmons are largely Landau damped in much of the relevant region of reciprocal space, making this linewidth a relatively minor issue. Decreasing Γ by a factor of 5, for example, reduces the scatter rates calculated in Sec. III by less than 5%. The final point regarding Γ is that the results discussed here are meant to illustrate the relative difference between scattering in parabolic and nonparabolic conduction bands; therefore, the plasmon linewidth is kept the same in both cases.

The function $\mathrm{Im}(1/\varepsilon)$ is calculated for n doped InAs at an electron density $N=1.5\times 10^{18}$ cm^{-3} and temperature $T_e=300$ K at various wave vectors. The nonparabolicity coefficient is set to $\alpha=1/0.36$ eV^{-1}, and Fermi levels appropriate for room temperature are used. The lattice component of the susceptibility described by Eq. (3) is also given a small linewidth (10^{11} s^{-1}) to facilitate numerical computation.[15] Rep-

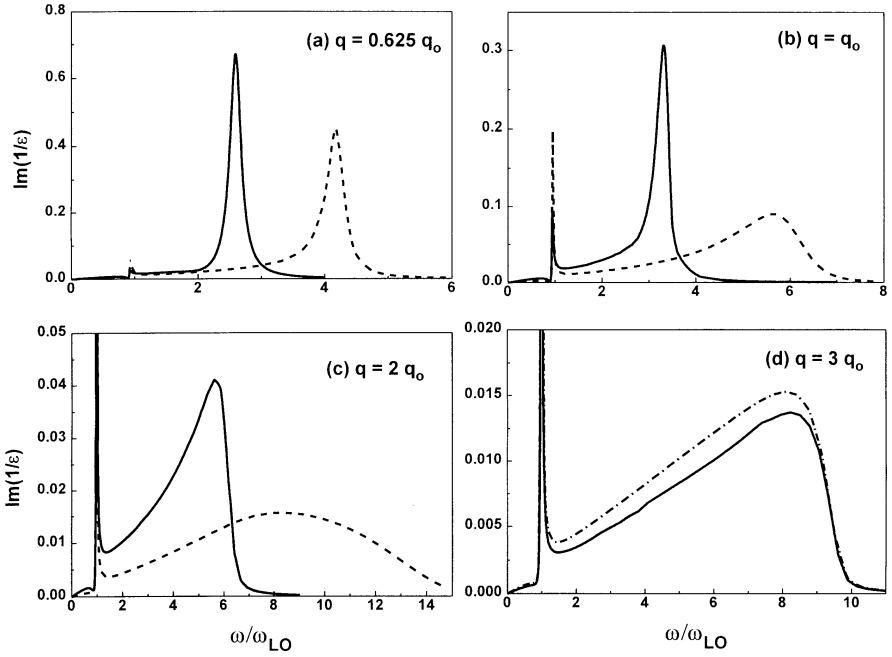

FIG. 3. The function $\mathrm{Im}(1/\varepsilon(q,\omega))$ describing the inelastic scattering spectrum of room temperature InAs with donor concentration $N_D = 1.5\times 10^{18}$ cm^{-3}. Plots (a)–(c) compare the nonparabolic calculation (solid line) to the parabolic case (dashed line) at increasing wave vectors. In (d), the nonparabolic calculation is shown for the case where the reduced overlap of conduction-band wave functions is included (solid line) and ignored (dash-dotted line).

resentative plots for parabolic (dashed lines) and nonparabolic bands (solid lines) are presented in Fig. 3 (note that there are identical curves at negative frequencies). At $q = 0.625 q_o$ [Fig. 3(a)], a distinct plasma mode (upper hybrid mode) is evident in both cases, where the different center frequencies reflect the nonparabolic nature of Eq. (11). Strong screening of the phonon mode (lower hybrid mode) at $\omega = \omega_{\mathrm{LO}}$ takes place. With increasing wave vector, the plasmon mode enters the regime where single-particle excitations can be supported and Landau damping of the mode commences.[8] The phonon mode simultaneously begins to emerge. Band dispersion affects the conditions for momentum conservation that define the single-particle excitation regime. Because the dispersion slope is much steeper in the parabolic case, the onset of appreciable Landau damping of plasmons occurs at smaller wave vectors. This is clearly revealed in the plots at $q = q_o$ [Fig. 3(b)] and $q = 2q_o$ [Fig. 3(c)]. Screening of the phonon mode, which is not well resolved in this series of figures, is discussed in Sec. IV.

At $q = 3q_o$ [Fig. 3(d)], the nonparabolic calculation (solid line) is compared to the same calculation except the Bloch function overlap factor [i.e., Eq. (5)] is set to unity (dash-dotted line), as was done by Dingrong *et al.*[2] The figure shows that, contrary to the assumption in Ref. 2, the overlap factor can be appreciably less than unity in narrow-gap semiconductors, particularly at large wave vectors.

III. INELASTIC SCATTERING

The hot-electron transistor has attracted considerable attention as a potential high-speed device.[16] The possibility of ballistic electron transport across an n-doped base is known to depend critically on inelastic scattering processes.[17,18] Hu and Das Sarma first considered the inelastic scattering of injected electrons in GaAs at nonzero temperature with accurate electron and dielectric functions.[19] Monoenergetic electrons, representing a δ-function perturbation of the carrier distribution, are injected into an n-doped region and allowed to interact with the scatter spectrum of the system that includes phonons, plasmons, and single-particle excitations. This approach was later refined by Sanborn *et al.* to include all four terms in the Boltzmann collision integral (i.e., scatter-out and scatter-in components) that are particularly important for electrons injected near the Fermi energy.[20] These efforts assumed a parabolic conduction band, which is entirely appropriate for GaAs. For many devices, however, collisonless transport is desired in thin layers of InAs, where complications from nonparabolicity are likely to occur. Lee[21] and later Krishnamurthy and co-workers[22,23] made allowances for nonparabolicity in their analysis of ballistic transport in various semiconductors including InAs, but neglected the electron-electron interaction. It is included here via the Lindhard function developed in Sec. II.

The calculational framework of Ref. 20 is used, modified for conduction-band nonparabolicity. The two scatter-in terms are

$$\frac{1}{\tau_{\mathrm{in}}(E)} = \frac{2\sqrt{2m}e^2}{\hbar^2\pi\sqrt{\gamma(E)}}\int_0^\infty \frac{dq}{q} I^2_{\mathbf{k},\mathbf{k}\pm\mathbf{q}} \int_{\hbar\omega_{\min}}^{\hbar\omega_{\max}} d(\hbar\omega) \times[1+2\alpha(E\pm\hbar\omega)]f(E\pm\hbar\omega) \times\left(N_q(\omega)+\frac{1}{2}\pm\frac{1}{2}\right)\mathrm{Im}\left(\frac{1}{\varepsilon(q,\omega)}\right), \tag{15a}$$

and for the scatter-out processes:

$$\frac{1}{\tau_{\text{out}}(E)} = \frac{2\sqrt{2m}e^2}{\hbar^2\pi\sqrt{\gamma(E)}} \int_0^\infty \frac{dq}{q} I^2_{\mathbf{k},\mathbf{k}\pm\mathbf{q}} \int_{\hbar\omega_{\min}}^{\hbar\omega_{\max}} d(\hbar\omega) \times[1+2\alpha(E\pm\hbar\omega)][1-f(E\pm\hbar\omega)] \times\left(N_q(\omega)+\frac{1}{2}\mp\frac{1}{2}\right)\text{Im}\left(\frac{1}{\varepsilon(q,\omega)}\right). \quad (15b)$$

The lattice and electrons are taken to be in thermal equilibrium and their common temperature is used in the Planck distribution function N_q. The $\pm$ sign refers to absorption and emission, respectively. The overlap factors are given by Eq. (5) with $E_{\mathbf{k}}$ replaced by E, the energy of the injected electron. All four terms in Eq. (15) add to give the total scatter rate. The limits on the inner integral are obtained from momentum conservation in the golden rule formulation of the scattering probability.[7] For absorption this gives:

$$\hbar\omega_{\max,\min} = \left(\frac{1+2\alpha E}{2\alpha}\right)\left(-1+\left\{1+\frac{4\alpha\hbar\omega_{\text{LO}}}{(1+2\alpha E)^2}\frac{q}{q_0} \times\left[\frac{q}{q_0}\pm 2\left(\frac{\gamma(E)}{\hbar\omega_{\text{LO}}}\right)^{1/2}\right]\right\}^{1/2}\right) \quad (16a)$$

and for emission the limits are

$$\hbar\omega_{\max,\min} = \left(\frac{1+2\alpha E}{2\alpha}\right)\left(1-\left\{1+\frac{4\alpha\hbar\omega_{\text{LO}}}{(1+2\alpha E)^2}\frac{q}{q_0} \times\left[\frac{q}{q_0}\pm 2\left(\frac{\gamma(E)}{\hbar\omega_{\text{LO}}}\right)^{1/2}\right]\right\}^{1/2}\right) \quad (16b)$$

where it is understood that the integration range is always positive ($\hbar\omega \geq 0$). The procedure used here is to calculate $\text{Im}(1/\varepsilon)$ separately, and then evaluate the integrals in Eq. (15). Results obtained for room temperature InAs with the complete nonparabolic treatment (solid line) and parabolic conduction band (dashed line) are depicted in Fig. 4 for two different donor densities. The InAs material parameters are taken as $m=0.023m_o$, $\hbar\omega_{\text{LO}}=0.03$ eV, $\varepsilon_0=14.55$, and $\varepsilon_\infty=11.8$. For all cases considered, a minimum scatter rate is obtained when the injected electrons have energy close to the Fermi level, in agreement with previous calculations[20] and measurements[24,25] made with GaAs. Note the shift of Fermi level to lower energy that occurs in the (more realistic) nonparabolic treatment of the conduction band. It is also found that the minimum scatter rate of $5-7\,\text{ps}^{-1}$ in InAs is approximately two times smaller than calculated by Sanborn *et al.* for comparably doped GaAs ($N=8\times10^{17}$ cm^{-3}).[20] This supports the earlier conclusion reached by Levi *et al.* who employed a much simpler model of scattering in InAs and GaAs.[26] They proposed that the inelastic scattering rate would be reduced with semiconductors having a lower density of conduction-band states compared to GaAs. Our calculations confirm this.

Figure 4 demonstrates the significance of the density of states in inelastic scattering. At the lighter doping density of 5×10^{17} cm^{-3} (top plot), the nonparabolic Fermi level resides at a relatively low energy in the conduction band ($E_F=0.068$ eV) where deviations from parabolicity are not pronounced (see Fig. 1). The scattering rates differ by roughly

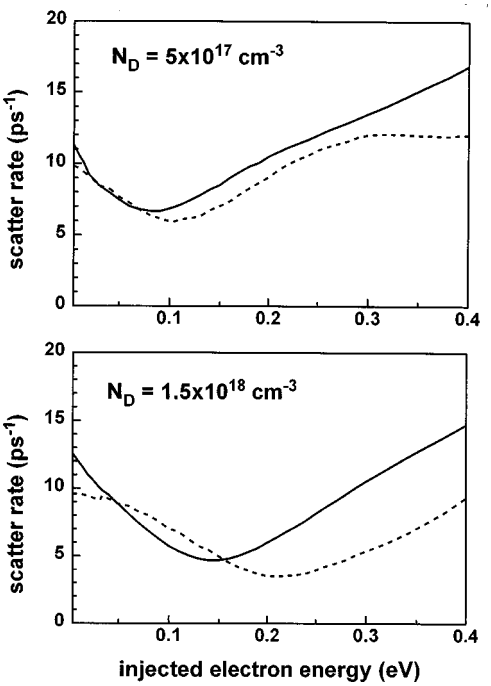

FIG. 4. Inelastic scatter rates of electrons injected into a bulk, room-temperature InAs at two different doping concentrations. The solid lines are obtained for a nonparabolic band, and the dashed lines correspond to the parabolic situation. In all cases, minimum scattering occurs in the immediate vicinity of the respective Fermi energies.

15% at energies immediately above the Fermi minimum. When the doping increases to 1.5×10^{18} cm^{-3} (lower plot), the Fermi level moves higher in the band ($E_F=0.145$ eV), where the nonparabolic density of states is 1.8 times larger than at the Fermi level in a parabolic band ($E_F=0.2055$ eV). In this case, the parabolic and nonparabolic scatter rates differ by about a factor of 2 for electrons injected above the Fermi level. The increased density of states as well as greater plasmon scattering in a nonparabolic conduction band, however, do not significantly degrade the potential for ballistic transport in bulk, room-temperature InAs when compared to GaAs.

Room-temperature operation of a unipolar ballistic electron transistor was first demonstrated by Levi and Chiu using a 100-Å n-doped InAs base layer, where quantum confinement is important,[27] and such devices continue to be an active area of research.[28–31] This paper is restricted to bulk semiconductor scattering; modification to accommodate the situation found in these devices—transport in the confined direction—is a difficult problem. In addition to the two-dimensional (2D) electron gas, scattering between subbands and the possibility of confined phonon modes must be addressed. Whether the 3D results presented here provide an upper limit estimate for scattering in strongly confined devices is not clear. The reduced density of 2D states, however, is obviously an advantage in vertical transport, as noted in Ref. 26. Extension of the present analysis to transport in the plane of a quantum well, with the assumptions of 3D phonons and electrons remaining in a single subband, would appear to be an easier task.[32]

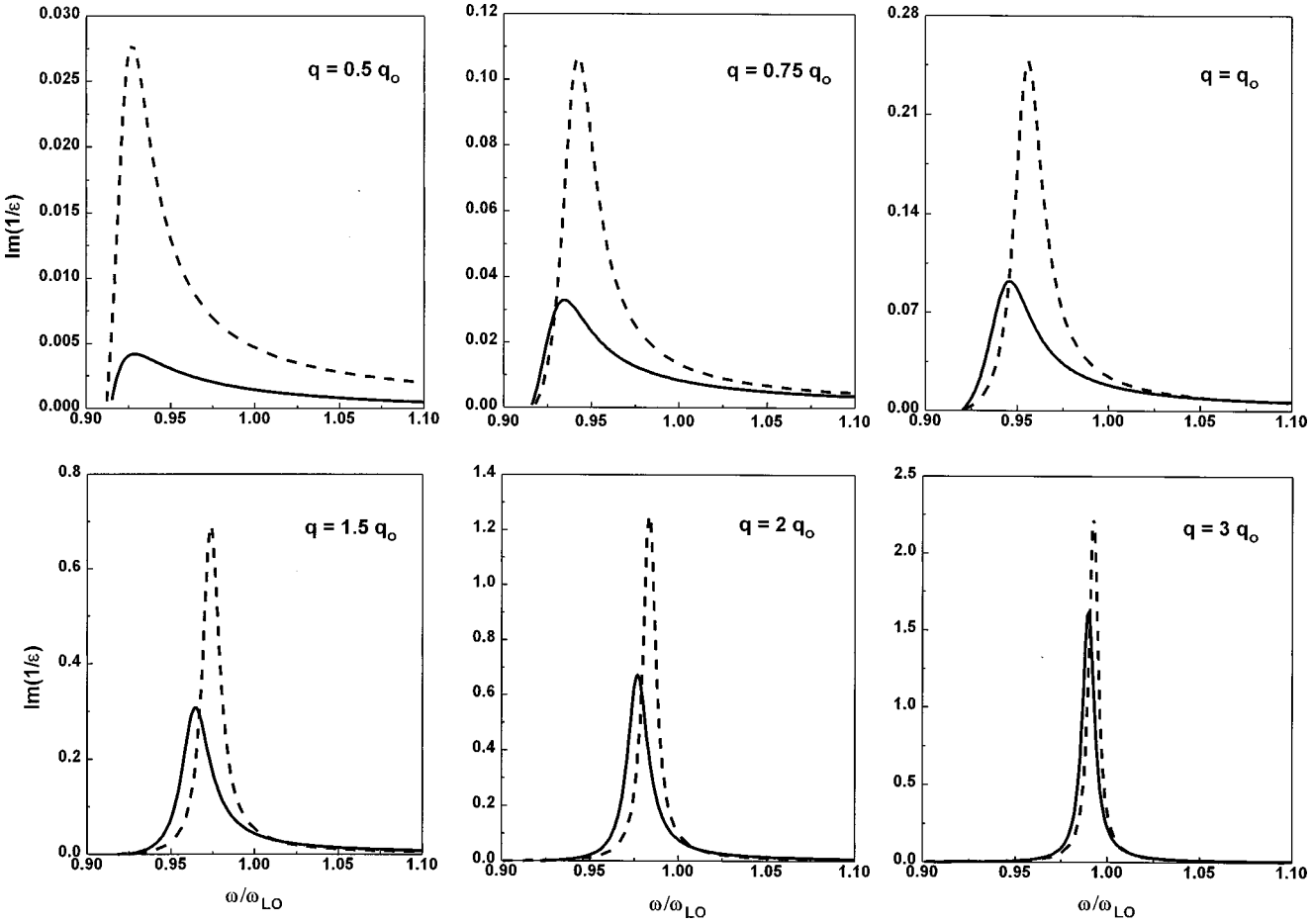

FIG. 5. The function $\mathrm{Im}(1/\varepsilon(q,\omega))$ in the frequency region of the phononlike mode for nonparabolic (solid lines) and parabolic (dashed lines) treatments of the conduction band at six different values of the momentum wave vector. The calculations are for InAs with a donor density of 1.5×10^{18} cm^{-3} and an electron temperature of 300 K. Note that the ordinate scale changes by almost two orders of magnitude in this sequence of figures. The strong reduction of mode strength that occurs in both calculations at small wave vectors is caused by plasma screening.

IV. HOT-ELECTRON COOLING

Cooling of hot-carrier distributions has been an important topic in semiconductor physics for decades. Most of the attention, however, has focused on medium and wide-gap materials where conduction-band nonparabolicity can be safely neglected. Conwell and Vassell first tackled the problem of LO-phonon scattering in a nonparabolic band,[33] but their calculations did not account for wave-function overlap and dynamic screening. These factors are included here to provide a more general description of the carrier relaxation process. It is important to point out that the problem as formulated here deals with a quasiequilibrium distribution of hot electrons losing energy by emission of optical phonons described by the Planck function with the temperature of the cold lattice, as is often encountered in ultrafast optical experiments. There is no external field present. Since a thermalized distribution of electrons is assumed (with temperature greater than the lattice), cooling via electron-electron interactions is ignored. The electrons affect the energy-loss rate indirectly, however, by screening the LO-phonon potential and Pauli blocking.

The nature of the random-phase approximation permits the lattice contribution to be isolated from the total dielectric function given by Eq. (2). By comparing the reciprocal dielectric function with and without the lattice term [i.e., Eq. (3)], the dynamically screened phonon mode can be obtained by simple subtraction. Results of this procedure are displayed in Fig. 5, where the phonon mode of InAs is shown at various wave vectors. In this calculation, heavy n doping ($N_D=1.5\times10^{18}$ cm^{-3}; $T_e=300$ K) provides an illustration of screening with parabolic (dashed line) and nonparabolic (solid lines) conduction bands. The plasmonlike mode occurs at higher frequency (cf. Fig. 3), and is not shown for clarity. What is evident is that nonparabolicity causes a distinct reduction of the phonon mode (i.e., increased screening) in the range $q<3q_o$. The reason for this is the same as discussed in Sec. II: a smaller curvature of the nonparabolic band extends the onset of Landau damping to larger wave vectors. The electron-electron interaction exhibits collective behavior outside this regime, leading to strong screening of the phonon potential. It is also worth noting that neglecting the overlap terms [Eq. (5)] causes screening to be overestimated in a nonparabolic conduction band for wave vectors larger than $q\approx1.5q_o$.

Figure 5 shows that the frequency of the phononlike mode is well approximated by that of the longitudinal-phonon oscillations (ω_{LO}), except at very small wave vectors where the mode is heavily screened and not well defined. The strength of this phonon mode at each value of q is obtained

by integrating $\mathrm{Im}(1/\varepsilon)$ over its narrow-frequency linewidth and then setting the scatter quanta energy to $\hbar\omega_{\mathrm{LO}}$. This approximation reduces the double integration needed in Sec. III to just one, and makes the cooling rate calculations comparatively simpler. The energy-loss rate for electrons at energy E is obtained from the *difference* of the following two components representing phonon absorption and emission:

$$\left(\frac{dE}{dt}\right)_{\mathrm{abs,emiss}} = \frac{2\sqrt{2m}\hbar\omega_{\mathrm{LO}}e^2}{\hbar^2\pi}\int_{-1}^{1} d(\cos\vartheta)\sqrt{\gamma(E\pm\hbar\omega_{\mathrm{LO}})}$$
$$\times[1+2\alpha(E\pm\hbar\omega_{\mathrm{LO}})]\,\frac{[1-f(E\pm\hbar\omega_{\mathrm{LO}})]\left(N_q(\omega_{\mathrm{LO}})+\frac{1}{2}\mp\frac{1}{2}\right)\mathrm{Im}\left(\frac{1}{\varepsilon(q,\omega_{\mathrm{LO}})}\right)I^2_{\mathbf{k},\mathbf{k}\pm\mathbf{q}}}{\gamma(E)+\gamma(E\pm\hbar\omega_{\mathrm{LO}})-2\sqrt{\gamma(E)\,\gamma(E\pm\hbar\omega_{\mathrm{LO}})}\cos\vartheta}, \tag{17}$$

where $\cos\vartheta$ is defined by Eq. (6); the vector subscripts are omitted here for brevity. The $\pm$ sign denotes phonon emission and absorption, respectively. The emission term is zero of course, unless $E>\hbar\omega_{\mathrm{LO}}$. As already noted, the reciprocal dielectric function is computed separately as a function of q and then integrated over frequency. The angular dependence necessary to integrate $\mathrm{Im}[1/\varepsilon(q,\omega_{\mathrm{LO}})]$ in Eq. (17) is obtained from momentum conservation in a nonparabolic band:

$$q = q_o\left(\frac{\gamma(E)+\gamma(E\pm\hbar\omega_{\mathrm{LO}})-2\sqrt{\gamma(E)\,\gamma(E\pm\hbar\omega_{\mathrm{LO}})}\cos\vartheta}{\hbar\omega_{\mathrm{LO}}}\right)^{1/2}, \tag{18}$$

where the $\pm$ sign again represents absorption and emission of phonons. The $\cos\vartheta$ dependence in the wave function overlap terms is explicit in Eq. (5).

The electron cooling rate due to dynamically screened LO-phonon emission (and absorption) is now applied to n-type InAs with conditions corresponding to the experiments of Elsaesser *et al.*[34] An infrared laser pulse with photon energy much less then the semiconductor band gap ($\lambda = 6.5\ \mu$m, $t_p = 8$ ps) excites conduction electrons in heavily doped, bulk InAs ($N_D = 1.5\times10^{18}\ \mathrm{cm}^{-3}$) held at a lattice temperature of 70 K. Free-carrier absorption (photon-electron-phonon scattering) heats the distribution to a temperature well above the lattice ($\sim$550 K), and is then used to monitor cooling. Because of the high donor density, complications from valence-band holes are negligible. A much longer decay than expected from screened phonon emission was observed and suggested the presence of the phonon bottleneck, which is known to inhibit carrier cooling in GaAs.[35]

The cooling calculations used in Ref. 34 assumed a parabolic conduction band and Thomas-Fermi screening. In Fig. 6, the energy-loss rate due to LO phonons is plotted for dynamic screening in a nonparabolic band (dash-dotted line), dynamic screening in a parabolic band (solid line), and static Thomas-Fermi screening in a parabolic band (dashed line). For purposes of comparison, hot-phonon effects have been ignored. The plotted loss rates are also averaged over a Fermi-Dirac distribution, so they can be displayed as a function of electron temperature.[36] As expected, the degenerate Thomas-Fermi approach provides an excellent representation of the full dynamic treatment of a parabolic band at low electron temperature. When nonparabolicity is included, however, the cooling rate increases by about a factor of 2. This is contrary to expectations from screening considerations alone—as revealed by Fig. 5, the phonon mode is always weaker in a nonparabolic band at equivalent wavevector positions. The faster cooling rate can be directly attributed to the higher density of states available in a nonparabolic conduction band. As was the case in Sec. III, differences in the density of states appear to be the dominant parameter when comparing inelastic scattering of degenerate electron distributions in parabolic and nonparabolic conduction bands.

A complete description of the data in Ref. 34 requires a time-dependent analysis that includes hot phonons as well as dynamic screening applied to free-carrier absorption. The latter issue is a formidable problem when both nonparabolicity and high doping concentrations are involved (cf. Ref. 37), and is beyond the scope of this paper. It can be concluded, however, that even with the more accurate calculation of cooling in a nonparabolic band presented here, an additional mechanism such as phonon reabsorption by the hot electrons as proposed in Ref. 34 is necessary to explain the relatively slow decay rate the authors observed in their experiments

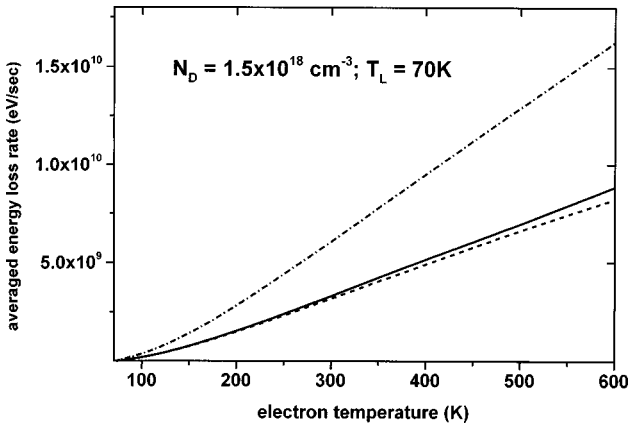

FIG. 6. Cooling rate of a hot, electron-donor ion plasma in InAs averaged over a Fermi-Dirac distribution as a function of electron temperature. The curves correspond to dynamic screening in a nonparabolic band (dash-dotted line), dynamic screening in a parabolic band (solid line), and static Thomas-Fermi screening in a parabolic band (dashed line).

with InAs. This is clear from Fig. 6, where the cooling rate in a nonparabolic band (assuming equilibrium phonon distributions) is faster than the parabolic case.

V. SUMMARY

The Lindhard dielectric function describing the electron-electron interaction was evaluated numerically for narrow-gap semiconductors including nonzero temperature, Fermi-Dirac statistics, and conduction-band nonparabolicity. Coupling to LO phonons was incorporated in the random-phase approximation. The inelastic scatter spectrum $\mathrm{Im}(1/\varepsilon(q,\omega))$ can be substantially different when comparing a nonparabolic to parabolic conduction band at the same carrier density and temperature. The reduced dispersion of a nonparabolic band dictates that the region of single particle excitations—the Landau damping regime for collective oscillations of the electron-donor ion plasma—occurs at higher wave vectors compared to a parabolic band. This changes the strength of both phonon and plasmon scattering.

A significant finding is that the increased density of states available at high energies in a nonparabolic conduction band is the primary factor leading to a larger electron scatter rate compared to the parabolic case. Changes to the inelastic scatter spectrum due to nonparabolicity appear to be of lesser importance. Even with an increased probability for deleterious collisions introduced by nonparabolicity, InAs compares favorably to GaAs in ballistic transport device applications.

ACKNOWLEDGMENTS

The authors acknowledge helpful dialogue with Barbara Sanborn and Professor David Ferry. M.P.H. was supported by the Alexander von Humboldt Foundation.

*Also with USAF Research Laboratories (PL/LIDD), Albuquerque, New Mexico 87117.

†Present address: Siemens AG, Siemensdamm 60–62, Berlin D-13627, Germany.

[1] D. K. Ferry and R. O. Grondin, *Physics of Submicron Devices* (Plenum, New York, 1991).

[2] Qian Dingrong, L. Liu, W. Szuszkiewicz, and W. Bardyszewski, Phys. Rev. B **44**, 5540 (1991).

[3] B. R. Nag, *Electron Transport in Compound Semiconductors* (Springer-Verlag, Berlin, 1980).

[4] David Yevick and Witold Bardyszewski, Phys. Rev. B **39**, 8605 (1989).

[5] Jeff F. Young and Paul J. Kelly, Phys. Rev. B **47**, 6316 (1993).

[6] Michael Woerner and Thomas Elsaesser, Phys. Rev. B **51**, 17 490 (1995).

[7] M. Kim, A. Das, and S. Senturia, Phys. Rev. B **18**, 6890 (1978).

[8] B. K. Ridley, *Quantum Processes in Semiconductors* (Clarendon, Oxford, 1993).

[9] W. G. Spitzer and H. Y. Fan, Phys. Rev. **106**, 882 (1957).

[10] Manuel Cardona, Phys. Rev. **121**, 752 (1961).

[11] P. Lugli and D. Ferry, Physica B **117**, 251 (1983).

[12] P. Lugli and D. Ferry, Appl. Phys. Lett. **46**, 594 (1985).

[13] K. Kral, Phys. Rev. B **50**, 7988 (1994).

[14] N. D. Mermin, Phys. Rev. B **1**, 2362 (1970).

[15] D. K. Ferry, Phys. Rev. B **10**, 4277 (1974).

[16] N. Yokoyama, H. Ohnishi, T. Mori, M. Takatsu, S. Muto, K. Imamura, and A. Shibatomi, in *Hot Carriers in Semiconductor Nanostructures*, edited by J. Shah (Academic, Boston, 1992).

[17] P. Lugli and D. Ferry, IEEE Electron Device Lett. **6**, 25 (1985).

[18] Elastic scattering due to ionized impurities is discussed in Refs. 22, 23, 25, and 26. It is only important for small injected electron energy.

[19] Ben Yu-Kuang Hu and S. Das Sarma, Phys. Rev. B **44**, 8319 (1991); **49**, 7833 (1993).

[20] B. A. Sanborn, Ben Yu-Kuang Hu, and S. Das Sarma, Phys. Rev. B **49**, 7767 (1994).

[21] Johnson Lee, J. Appl. Phys. **52**, 4676 (1981).

[22] S. Krishnamurthy, A. Sher, and A. B. Chen, Appl. Phys. Lett. **52**, 468 (1988).

[23] S. Krishnamurthy, M. A. Berding, A. Sher, and A. B. Chen, J. Appl. Phys. **63**, 4540 (1988).

[24] A. F. J. Levi, J. R. Hayes, P. M. Platzmann, and W. Wiegmann, Phys. Rev. Lett. **55**, 2071 (1985).

[25] J. R. Hayes and A. F. J. Levi, IEEE J. Quantum Electron. **QE-22**, 1744 (1986).

[26] A. F. J. Levi, J. R. Hayes, and R. Bhat, Appl. Phys. Lett. **48**, 1609 (1986).

[27] A. F. J. Levi and T. H. Chiu, Appl. Phys. Lett. **51**, 984 (1987).

[28] T. H. Chiu and A. F. J. Levi, Appl. Phys. Lett. **55**, 1891 (1989).

[29] K. Funato, K. Taira, F. Nakamura, and H. Kawai, Appl. Phys. Lett. **59**, 1714 (1991).

[30] K. Taira, K. Funato, F. Nakamura, and H. Kawai, J. Appl. Phys. **69**, 4454 (1991).

[31] J. Walachova, J. Zelinka, J. Vanis, D. H. Chow, J. N. Schulman, S. Karamazov, M. Cukr, P. Zich, J. Kral, and T. C. McGill, Appl. Phys. Lett. **70**, 3588 (1997).

[32] S. Das Sarma, in *Hot Carriers in Semiconductor Nanostructures* (Ref. 16).

[33] E. M. Conwell and M. O. Vassell, Phys. Rev. **166**, 797 (1968).

[34] T. Elsaesser, R. J. Baüerle, and W. Kaiser, Phys. Rev. B **40**, 2976 (1989).

[35] Jagdeep Shah, Solid-State Electron. **32**, 1051 (1989).

[36] K. Seeger, *Semiconductor Physics* (Springer-Verlag, New York, 1989).

[37] Jerzy Mycielski and Andrzej Mycielski, Phys. Rev. B **18**, 1859 (1978).